

Data analysis and the metric evolution of hypergraphs

Dalma Bilbao^{1,3}, Hugo Aimar^{1,3}, and Diego M. Mateos^{1,2,3,*}

¹Consejo Nacional de Investigaciones Científicas y Técnicas (CONICET), Argentina.

²Facultad de Ciencia y Tecnología. Universidad Autónoma de Entre Ríos (UADER). Oro Verde, Entre Ríos, Argentina.

³Instituto de Matemática Aplicada del Litoral (IMAL-CONICET-UNL), CCT CONICET, Santa Fé, Argentina.

*Corresponding author: Diego M. Mateos, mateosdiego@gmail.com

Abstract

In this paper we aim to use different metrics in the Euclidean space and Sobolev type metrics in function spaces in order to produce reliable parameters for the differentiation of point distributions and dynamical systems. The main tool is the analysis of the geometrical evolution of the hypergraphs generated by the growth of the radial parameters for a choice of an appropriate metric in the space containing the data points. Once this geometric dynamics is obtained we use Lebesgue and Sobolev type norms in order to compare the basic geometric signals obtained.

Keywords— Hypergraphs, Metrics, Distances, Dynamical Systems

1 Introduction

As never before in history, there are large volumes of data available today, for example, internet data, engineering signals or medical images. It is often difficult to extract valuable information from these datasets using traditional statistical methods. In addition, in most cases, we want to know the relationship between the components of the data, which is usually taken as a pairwise relationship. It is therefore natural to approach the problem from the point of view of graphs. However, in most real systems, the relationship between the components is not bipartite. In these cases, what is usually done is to compress these complex relationships between pairs, without considering that this generates a loss of valuable information. To overcome this problem, Berge developed the hypergraph theory [1, 2], which represents the multiple component relationships in a system. Hypergraph theory has been used in recent years in multiple applications from signal analysis [3, 4], study of chemical reaction networks [5, 6] to biological networks [7, 8]. It has also been used in the study of clinical pathologies such as cardiac problems [9], neurodegenerative diseases [10] and epilepsy detection [11]. Numerous applications of hypergraphs can be found in the area of machine learning, from image classification [12], use of genetic algorithms [13], to detection of covid-19 in CT images. For a more in-depth review of hypergraph applications, see [14].

In this paper, we use hypergraph theory to study the metric structure of a data set. For this we use the idea of filtration coming from algebraic topology. This implies not having a fixed hypergraph for the data, but a set of hypergraphs which are formed based on a variable parameter. The idea is that dynamic hypergraph approach provides a powerful tool to infer robust qualitative and quantitative information about the structure of the data. This is done by taking as a basis a finite set of data –which can be points, signals, distributions or images, among others– with a notion of distance or similarity between them. This distance can be induced by the metric in the ambient space (e.g. the Euclidean metric when the data are embedded in \mathbb{R}^n) or come as an intrinsic metric defined by a pairwise distance matrix. The definition of the metric on the data is usually guided by the application. Once we have chosen the metric space to work with, we define balls of radius r centered at each data point we have. Subsequently, we increase the radius of the balls centered at any data point until we cover the entire set of the data. The data that fall into the balls are the ones that form the hyperedges of the hypergraphs. For each radius, we generate the associated hypergraph and apply a quantifier. This filtering method allows us to study the relationships between the data that remain unchanged as the radius changes. Different data topologies will present different quantifier values, allowing us to distinguish between different systems. In particular, in this study, we used five sets of points in the space generated with different distributions and four sets of data coming from dynamical systems. The data were studied in five different metric spaces. In all cases, the filtering method was applied to generate the dynamic of the hypergraphs. The number of hyperedges was computed as a quantifier for each hypergraph as a function of the radius r and the L^1 -norm and the Sobolev discrete seminorm were calculated for each generated curve in order to collapse all the information into a single number. The results obtained show that it is possible to differentiate all the data sets analysed, both point distributions and dynamical systems. However, these results depend on the metric space used to generate the distance matrix of each system. This freedom in the choice of the underlying metric in the space containing the data set provides flexibility and robustness to the method.

2 Graph, hypergraphs and covering.

2.1 The general setting.

Let χ be a set. We may think of χ as a very large set containing all our possible data points. χ can be the set of points in some euclidean space \mathcal{R}^n or even some functional space when our “data points” are signals or images. In classical mathematical analysis such spaces can be taken to be Hilbert spaces, Banach spaces or even metric space. For the sake of generality, which will allow us to consider non symmetric “metrics” such as the Kullback-Leibler divergence, we shall not even assume that χ is a metric space. Instead, we shall start considering a much more general metric-like structure an χ .

Definition 1 A function $\delta : \chi \times \chi \rightarrow \mathbb{R}_0^+$ shall called a “protometric” if δ satisfies $\delta(x, y) = 0$ if and only if $x = y$. The δ -ball centered at $x \in \chi$ with radius $r > 0$ is defined by: $\mathcal{B}_\delta(x, r) = \{ y \in \chi : \delta(x, y) < r \}$.

Observe that with the above definition of protometric, in general $\mathcal{B}_\delta(x, r)$ does not coincide with the set $\{ y \in \chi : \delta(x, y) < r \}$ since δ may not be symmetric. Of course every metric in χ is a protometric. Recall that a metric d in χ satisfies the additional properties:

- $d(x, y) = d(y, x)$ for every choice of x and y in χ , and
- $d(x, z) \leq d(x, y) + d(y, z)$ for every choice of x, y and z in χ .

Let $\mathcal{V} = \{x_1, x_2, \dots, x_n\}$ be a finite sample of points in (χ, d) . For any positive r and every $i = 1, 2, \dots, n$; set

$$e_i(r) = \mathcal{B}_\delta(x_i, r) \cap \mathcal{V} = \{x_j \in \mathcal{V} : \delta(x_i, x_j) < r\},$$

to denote the hyperedge centered at x_i with radius $r > 0$.

Set $\mathcal{E}(r)$ to denote the family of all the hyperedges with radius $r > 0$ fixed. Notice that the number of hyperedges in $\mathcal{E}(r)$ is some number $m(r)$ between one and n .

Proposition 1 For each $r > 0$, the couple $(\mathcal{V}, \mathcal{E}(r))$ is an hypergraph with the additional property $x_i \in e_i(r)$ for every $i = 1, 2, \dots, n$.

If we consider this hypergraph structure as a function of $r > 0$, we have some basic and elementary properties.

Proposition 2 Let $(\mathcal{V}, \mathcal{E}(r))$ as before. Then

- $e_i(r_1) \subset e_i(r_2)$ if $0 < r_1 \leq r_2 < \infty$;
- $e_i(r) = \{x_i\}$ if $0 < r \leq \min_j \delta(x_i, x_j)$;
- $e_i(r) = \mathcal{V}$ if $r > \max_j \delta(x_i, x_j)$.

In other words, we have a family of hypergraphs starting at the trivial isolated point of \mathcal{V} and finishing at the trivial full hypergraph whose only hyperedge is \mathcal{V} itself.

Now we can generate an adjacency $n \times n$ matrix $\mathcal{A}(r)$ associated to the hypergraph $(\mathcal{V}, \mathcal{E}(r))$ which is given by

$$\mathcal{A}(r) = \begin{pmatrix} 1 & \mathbb{I}_{e_2(r)}(x_1) & \dots & \mathbb{I}_{e_n(r)}(x_1) \\ \mathbb{I}_{e_1(r)}(x_2) & 1 & \dots & \mathbb{I}_{e_n(r)}(x_2) \\ \mathbb{I}_{e_1(r)}(x_3) & \mathbb{I}_{e_2(r)}(x_3) & \dots & \mathbb{I}_{e_n(r)}(x_3) \\ \vdots & \vdots & \ddots & \vdots \\ \mathbb{I}_{e_1(r)}(x_n) & \mathbb{I}_{e_2(r)}(x_n) & \dots & 1 \end{pmatrix} = \left(\mathbb{I}_{e_j(r)}(x_i) \right)_{\substack{i=1, \dots, n \\ j=1, \dots, n}}$$

while \mathbb{I}_θ is the indicator functional of θ , i.e $\mathbb{I}_\theta(x) = 1$ if $x \in \theta$ and $\mathbb{I}_\theta(x) = 0$ if $x \notin \theta$. Notice that (χ, d) is a metric space, then $\mathcal{A}(r)$ is symmetric for every $r > 0$. In fact, since $d(x, y) = d(y, x)$, we readily have that $\mathbb{I}_{e_j(r)}(x_i) = \mathbb{I}_{e_i(r)}(x_j)$, because $d(x_i, x_j) < r$ if and only if $d(x_j, x_i) < r$.

Notice also that for $r > 0$ fixed it could happen that $e_i(r) = e_j(r)$ for some $i, j \in \{1, 2, \dots, n\}$. In this case the repeated column of the matrix (hyperedges) are eliminated, resulting in a new matrix $n \times m(r)$ with $m(r) \leq n$ call incidence matrix \mathcal{I} . Figure 1 show an example of a hypergraph and it's incidence matrix associated.

Definition 2 Giving an incidence matrix $\mathcal{I}(r)$ $m(r) \times n$ associated to the hypergraph $(\mathcal{V}, \mathcal{E}(r))$ with $r > 0$, we define the degree of hyperedges $\Delta^e(r)$ as

$$\Delta^e(r) = m(r) \tag{1}$$

This measure will be used to characterise the hypergraphs generated for the different values of r .

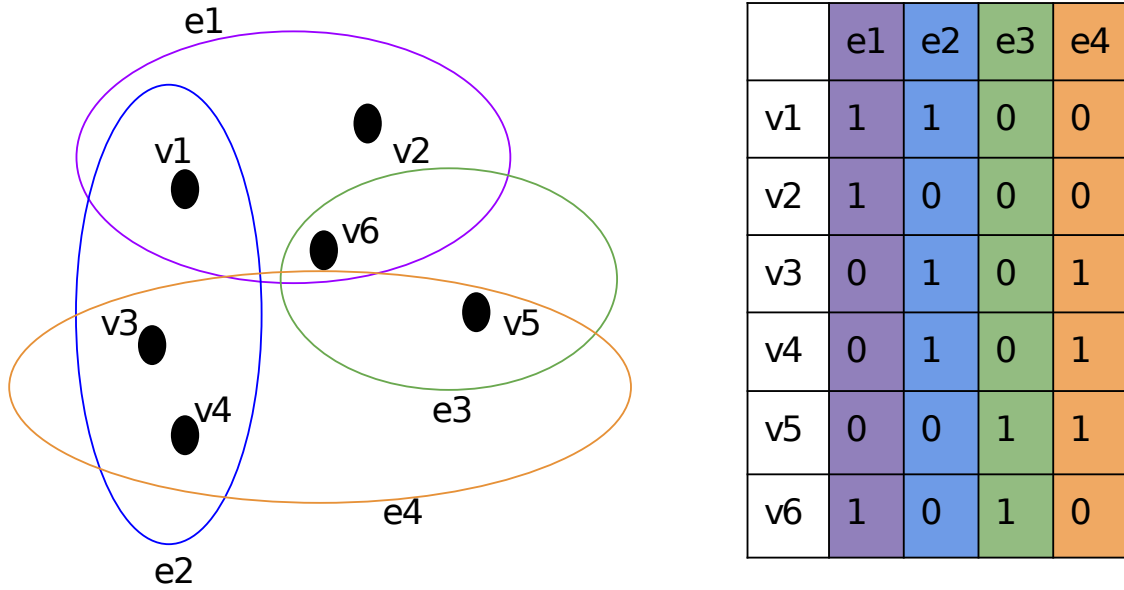


Figure 1: Incidence matrix for a hypergraph formed by 6 vertices and 4 hyperedges.

3 Methods

3.1 Data

In this paper, we used two types of data sets. The first one are sets of points in \mathbb{R}^3 generated under different distributions: i) Normal, ii) Uniform, iii) Poisson and generated with a specific structure iv) Lattice and v) Fractal (see Figure 2(top)). For each set, we generated 100 realizations of 1000 points each one. The second type of data set belongs to 3-dimensional chaotic systems with different topologies: i) Rossler map, ii) Complex Butterfly map, iii) Lorenz map and a iv) white noise (see figure 2 (bottom)). For each system, we generated 100 sequences of 10000 data each one, and then subsampled to 1000 data. All datasets generated are described in depth in Appendix A.

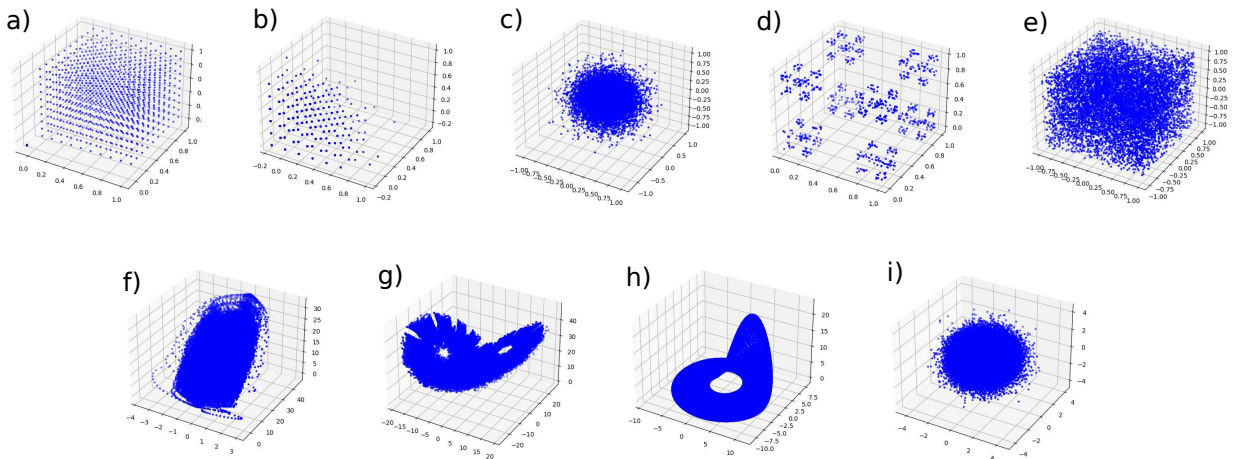


Figure 2: Examples of different set of data used in the analysis. Points distribution / arrays (top) a) Lattice, b) Poisson, c) Normal, d) Fractal and e) Uniform. Dynamical systems (bottom) f) Complex Butterfly, g) Lorenz map, h) Rossler map, i) White noise.

3.2 Basic Metrics

As we explained in Section 2, giving a set of points χ we can use a metric to measure the distance between all pairwise components of the set, giving a $n \times n$ distance matrix \mathcal{D}_χ . In the sets considered in this paper we used five different metrics that we proceed to define explicitly.

Definition 3 Giving a set of point $\chi \in \mathbb{R}^n$ with $\chi = \{\mathbf{x}_1, \dots, \mathbf{x}_m\}$ we define the component $i, j = 1, \dots, m$ with $j > i$ of the matrix distance \mathcal{D}_χ as:

1. *Euclidean:*

$$\mathcal{D}_\chi^{Ecu}(i, j) = \sqrt{\sum_{l=1}^n (\mathbf{x}_i^l - \mathbf{x}_j^l)^2}, \text{ where } \mathbf{x}_i = (x_i^1, \dots, x_i^n)$$

2. *Chebyshev:*

$$\mathcal{D}_\chi^{Cheb}(i, j) = \max_{l=1, \dots, n} |\mathbf{x}_i^l - \mathbf{x}_j^l|$$

3. *Cityblock:*

$$\mathcal{D}_\chi^{city}(i, j) = \sum_{l=1}^n |\mathbf{x}_i^l - \mathbf{x}_j^l|$$

4. *Minkowski:*

$$\mathcal{D}_\chi^{Mink}(i, j) = \left(\sum_{l=1}^n |\mathbf{x}_i^l - \mathbf{x}_j^l|^p \right)^{\frac{1}{p}}, \quad 1 \leq p < \infty$$

5. *Parabolic:*

$$\mathcal{D}_\chi^{Par}(i, j) = \max_{l=1, \dots, n} |\mathbf{x}_i^l - \mathbf{x}_j^l|^{\alpha_l} \text{ with } 0 < \alpha_l \leq 1, \quad l = 1, \dots, n.$$

3.3 Steps to built and characterise the hypergraphs $\mathcal{H}(r)$

Let us now proceed to summarise the algorithm used to analyse a set of data based on the characterization of hypergraph. Given a data set $\chi = \{x_1, \dots, x_m\}$ we generate and characterise the hypergraph associate to χ as follow, (see Figure 3).

Algorithm 1 Hypergraph filtration method

- 1: Define the distance d over the component of the set χ .
- 2: Build the distance matrix \mathcal{D}_χ .
- 3: For each $x \in \chi$ define a ball centred in x_i $\mathcal{B}(x_i, r)$ with $0 < r < 1$.
- 4: Build the matrix \mathcal{M} for each r as

$$\mathcal{M}_{i,j}(r) = \begin{cases} 1 & \text{if } d^k(x_i, x_j) \in \mathcal{B}(x_i, r) \\ 0 & \text{if } d^k(x_i, x_j) \notin \mathcal{B}(x_i, r) \end{cases} \text{ for } i, j = 1, \dots, m, \quad i < j.$$

- 5: Obtain the $n \times m(r)$, $m(r) \leq n$ incidence matrix $\mathcal{I}(r)$ eliminating the repeated columns of the matrix $\mathcal{M}(r)$.
 - 6: Compute the degree of hyperedges $\Delta^e(r)$
-

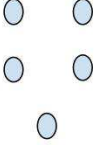
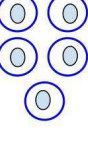
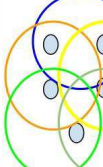
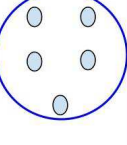
r	0	0,2	0,5	1
Hypergraph				
Δ^e	-	5	5	1

Figure 3: Steps to build and measure the feature Δ^e of the hypergraph for different values of r .

4 Results

We analysed the distributions of points and dynamical systems presented in Section 3.1 using the filtration algorithm propose in the Section 3.3. In Figure 4 and 5 we show the Hypergraph degree Δ^e vs r for distribution points and dynamical systems respectively. The straight line represent the mean value over 100 realisation and the shadow band is the standard deviation. Each subplot correspond a different distances used to obtain the hypergraph.

In Figure 4 it can be observed the results for the case of \mathbb{R}^3 data point distributions. We can see that the analysis of the number of hyperedges Δ^e for all the distance can clearly distinguish between the fives types of point distribution, being more remarkable the Chebyshev and Parabolic distance.

Particularly it is seen that for the isotropic metrics (\mathcal{D}^{Euc} , \mathcal{D}^{Cheb} , \mathcal{D}^{City} , \mathcal{D}^{Mink}), the lattice array starts with the number of hyperedges similar to the number of vertices, and remains constant until r approaches $r = 0.58$, where the number of hyperedges decreases until it reaches zero. Depending on the distance used, this decrease is not uniform, being fluctuating for the Euclidean and Minkowski, and stepwise for the Chebyshev and cityblock distance. On the other hand, for the parabolic distance, the behaviour is very different, starting with very low number of hiperedges $\Delta^e \sim 150$ and decaying to zero in ($r \sim 0.28$).

In the case of the Normal distribution, the number of hyperedges is similar to the number of vertices for small r . For $r \sim 0.06$ a drop in Δ^e is observed but it quickly recovers the initial values. Finally, there is a uniform drop in the number of hyper edges reaching zero for $r = 1$, this occurs for $r \sim 0.6$ in the symmetric distance and $r \sim 0.3$ for the parabolic distance.

Uniform distribution present a similar behaviour as the Normal distribution. However the uniform decrease in the number of hyperedges start before in $r \sim 0.6$ for all the metrics.

The Poisson distribution showing a higher data clusterization giving a lower number of hyperedges even for initial values of r . These values remain constant until $r \sim 0.06$ where decrease uniformly to zero. This behaviour occurs for all the metrics.

In the case of fractal distribution, the number of hyperedges depends strongly in the r values, and the behaviour of the curves is very different for the distinct metrics. Particularly, the Chebyshev and Parabolic distances showing constant periods with very low numbers of hyperedges alternating with peaks with high numbers Δ^e . Similar fluctuations are presented in the other metrics in the range between $0 < r \leq 0.7$, before $r \sim 0.7$ the Δ^e decay to zero, similar to the other distribution.

In the second instance, we analysed the dynamical systems presented in the Section 3.1. Figure 5 shows the analysis of the number of hyperedges vs r parameter for the dynamics system. For the Δ^e study, the Chebishev and Parabolic distance (with $\alpha^1 = 1$, $\alpha^2 = 1/2$, $\alpha^3 = 1/2$) are the best at differentiating the four dynamical system. On the other hand, the Euclidean distance could not see any differences between them. For the fives metrics, white noise starts with the similar number of hyperedges than vertices for small r and shows a drop in $r \sim 0.06$ but fast returns to original values. Then, remains with higher values of Δ^e until $r \sim 0.5$ for isotropic metrics and $r \sim 0.3$ for parabolic distances when decrease uniformly to zero in $r = 1$. For isotropic metrics Rossler map begin with $\Delta^e < N_{vert}$ but promptly increases near to the maximum at $r \sim 0.2$ and remaining until $r \sim 0.6$ then decay to zero. However, for the parabolic distance the behaviour of the curve is very difference decreasing very sharp at $r \sim 0.15$ and changing the slope at $r \sim 0.2$. Complex butterfly and Lorenz maps present a similar behaviour for the isotropic metrics except for Chebyshev where the slope changes a little between then. But for Parabolic distance the differences between this two chaotic maps are very remarkable. Similar situation we have for Lorenz map where the only distance that can clearly distinguish for the others dynamical systems is the parabolic distance.

4.1 Distance quantification

In the previous section, we saw that distinct distribution or dynamics could be differentiated on the base of the shapes of the curves traced by the function $\Delta^e(r)$. In this section, we quantified more accurately the result obtained with $\Delta^e(r)$. For that aim we used two metric, L^1 -norm (\mathcal{L}) [15] and the discrete Sobolev semi-norm of order 1 (\mathcal{S}). The L^1 -norm is defined as

$$\mathcal{L} = \sum_{i=1}^m |\Delta^e(r_i)|$$

and the Sobolev seminorm as:

$$\mathcal{S} = \sum_{i=2}^m \frac{|\Delta^e(r_i) - \Delta^e(r_{i-1})|}{r_i - r_{i-1}}.$$

The idea behind the use of these two metrics is the possibility to quantify the content of the curves by its area (\mathcal{L}) and the changes in their slopes (\mathcal{S})

Moreover, to measure a significant distance between two different systems we define the following pipeline. Having a group of curves $\mathcal{V} = \{\Delta^e(r)_1, \dots, \Delta^e(r)_n\}$ and $\hat{\mathcal{V}} = \{\Delta^e(\hat{r})_1, \dots, \Delta^e(\hat{r})_n\}$ corresponding with n realization of each system (for example n different white noises), we estimate the mean values $\mu(r)$ and standard deviation $\sigma(r)$ for each group.

Then, we calculate the distance $d^{\mathcal{V}, \hat{\mathcal{V}}}(r)$ between the two group as follows:

If $\sigma(r) < \hat{\sigma}(r)$ then

$$d^{\mathcal{V}, \hat{\mathcal{V}}}(r) = \begin{cases} (\mu(r) - \sigma(r)) - (\hat{\mu}(r) + \hat{\sigma}(r)) & \text{if } (\mu(r) - \sigma(r)) > (\hat{\mu}(r) + \hat{\sigma}(r)) \\ 0 & \text{if } (\mu(r) - \sigma(r)) \leq (\hat{\mu}(r) + \hat{\sigma}(r)) \end{cases}$$

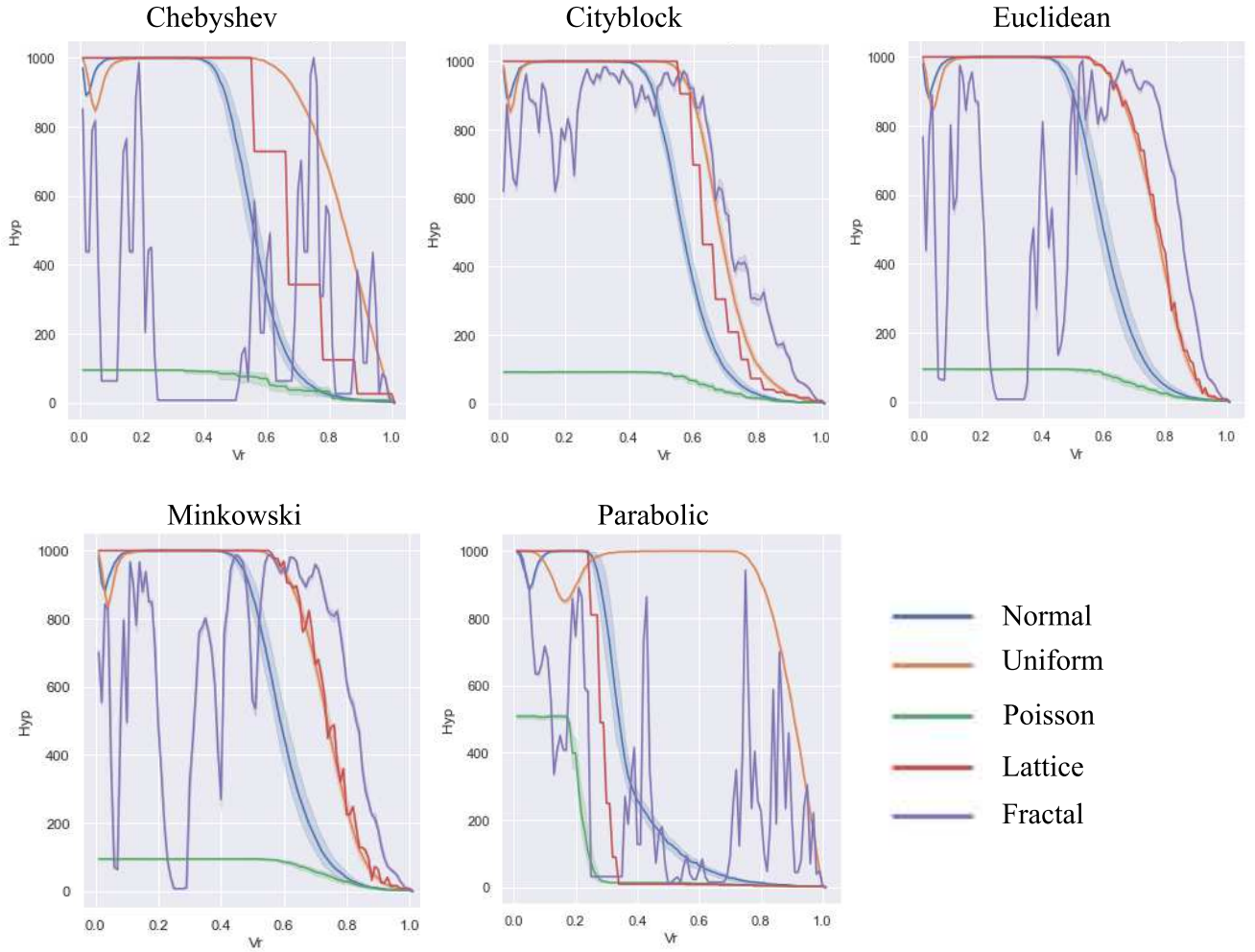


Figure 4: Analysis of the number of hyperedges versus parameter r , for \mathbb{R}^3 data points distribution. Each subplot represents the distance metric used to obtain the hypergraph.

or $\sigma(r) > \hat{\sigma}(r)$ then

$$d^{\nu, \hat{\nu}}(r) = \begin{cases} (\hat{\mu}(r) - \hat{\sigma}(r)) - (\mu(r) + \sigma(r)) & \text{if } (\hat{\mu}(r) + \hat{\sigma}(r)) > (\mu(r) - \sigma(r)) \\ 0 & \text{if } (\hat{\mu}(r) - \hat{\sigma}(r)) \leq (\mu(r) + \sigma(r)) \end{cases}$$

Finally we quantify the difference applying the two norms described before L^1 -norm and Sovolev semi-norm of order 1 to the distance vector $d^{\nu, \hat{\nu}}(r)$.

Table 1 shows the \mathcal{L} and \mathcal{S} mean and standard deviation values over Δ^e curves for the different points distribution. As we could saw in the figure 4, the Parabolic and Chebichev distance are the best metrics to differentiating the fives distribution -this is reflected in the wide distribution of \mathcal{L} and \mathcal{S} values in the table-. Cityblock and Euclidean distances could not discriminate well the five cases, and Minkowsky only can discern the distribution just for \mathcal{S} metric. For all the distances we can remark the high difference between fractal \mathcal{S} values array with the others distribution, this behaviour is not reflected in \mathcal{L} values. This facts reflects the fractal intrinsic character of the fractal. In table 3 and 4 we measure the distance \mathcal{L} and \mathcal{S} respectively between the distribution for the Parabolic distance (the other distances are shown in supplementary material). For \mathcal{L} values, Normal distribution and lattice are the most similar, and Poisson and uniform present the highest differences. In \mathcal{S} distance between Poisson and lattice become more similar, and the lattice and fractal have the highest distance .

For the dynamical systems, the \mathcal{L} and \mathcal{S} over Δ^e is presented in the table 2. In this case, the differentiation between systems is less clear than before. Chebyshev is the ones which shown significant difference \mathcal{L} and parabolic in \mathcal{S} values. Measuring the distances between the systems we can better appreciate their differences. For that we measure \mathcal{L} para el caso de la Chebyshev (table 5) and the \mathcal{S} for the parabolic case (6).

System	Distance	$\mathcal{L} (\mu \pm \sigma)$	$\mathcal{S} (\mu \pm \sigma)$
Lattice		68492±0	999±0
Fractal	Chebyshev	24364±125	10916±76
Normal		56053±3597	1209±17
Poisson		6579±539	96±4
Uniform		82944±329	1321±16
Lattice		65774±0	999±0
Fractal	Cityblock	66677±299	4835±205
Normal		58774±2463	1211±21
Poisson		6558±285	93±4
Uniform		69315±1205	1299±21
Lattice		74190±0	1527±0
Fractal	Euclidean	59941±301	8612±354
Normal		60763±2970	1229±18
Poisson		6584±648	109±6
Uniform		72448±1240	1341 ±24
Lattice		76850±0	1143±0
Fractal	Minkowsky	53260±361	9704±288
Normal		60521±2541	1241±23
Poisson		6744± 767	142±27
Uniform		60521±2541	1241±23
Lattice		285780 ±0	999±0
Fractal	Parabolic	29806±170	11558±76
Normal		39081±2689	1261±27
Uniform		87942±202	1335±21
Poisson		11729± 736	512± 11

Table 1: Mean values and standard deviation for the L^1 -Norm (\mathcal{L}) and Sobolev seminorm (\mathcal{S}) applied over the $\Delta^e(r)$ curves belong to the different 3D point distribution.

System	Distance	$\mathcal{L} (\mu \pm \sigma)$	$\mathcal{S} (\mu \pm \sigma)$
Complex Butterfly		49037± 626	1279±32
Lorenz map	Chebyshev	58370 ± 1042	1270±21
Rosler map		61935 ±1586	1322±40
White Noise		57755± 2228	1213±16
Complex Butterfly		60686±1056	1268±25
Lorenz map	Cityblock	61540±1044	1284±17
Rosler map		52628±1465	1260±16
White Noise		58183±2490	1217±15
Complex Butterfly		60133±818	1295±38
Lorenz map	Euclidean	63138±1582	1285±13
Rosler map		61426±1548	1323±48
White Noise		62095±1920	1247±14
Complex Butterfly		57854±668	1298±38
Lorenz map	Minkowsky	61012±1578	1290±24
Rosler map		62710±1909	1317±29
White Noise		60807±2289	1238±23
Complex Butterfly		61573± 13041	1340± 29
Lorenz map	Parabolic	39240± 992	1634± 62
Rosler map		39834± 1973	1501± 83
White Noise		39342 ± 2151	1265± 15

Table 2: Mean values and standard deviation for the L^1 -Norm (\mathcal{L}) and Sobolev seminorm (\mathcal{S}) applied over the $\Delta^e(r)$ belong to the different dynamical system.

	Lattice	Fractal	Normal	Poisson	Uniform
Lattice	0	23133	8460	16051	61770
Fractal	23133	0	23974	17676	57333
Normal	8460	23974	0	23243	48398
Poisson	16051	17676	23243	0	74607
Uniform	61770	57333	48398	74607	0

Table 3: \mathcal{L} distance matrix for parabolic metric between 3D points distribution.

	Lattice	Fractal	Normal	Poisson	Uniform
Lattice	0	11928	1597	1487	2225
Fractal	11928	0	11195	11134	11414
Normal	1597	11195	0	1639	2384
Poisson	1487	11134	1639	0	1857
Uniform	2225	11414	2384	1857	0

Table 4: \mathcal{S} distance matrix for parabolic metric between 3D points distribution.

	White Noise	Complex Butterfly	Lorenz	Rosler
White Noise	0	4989	797	4137
Complex Butterfly	4989	0	6975	10653
Lorenz	797	6975	0	2468
Rosler	4137	10653	2468	0

Table 5: \mathcal{L} distance matrix for Chebyshev metric between dynamical system.

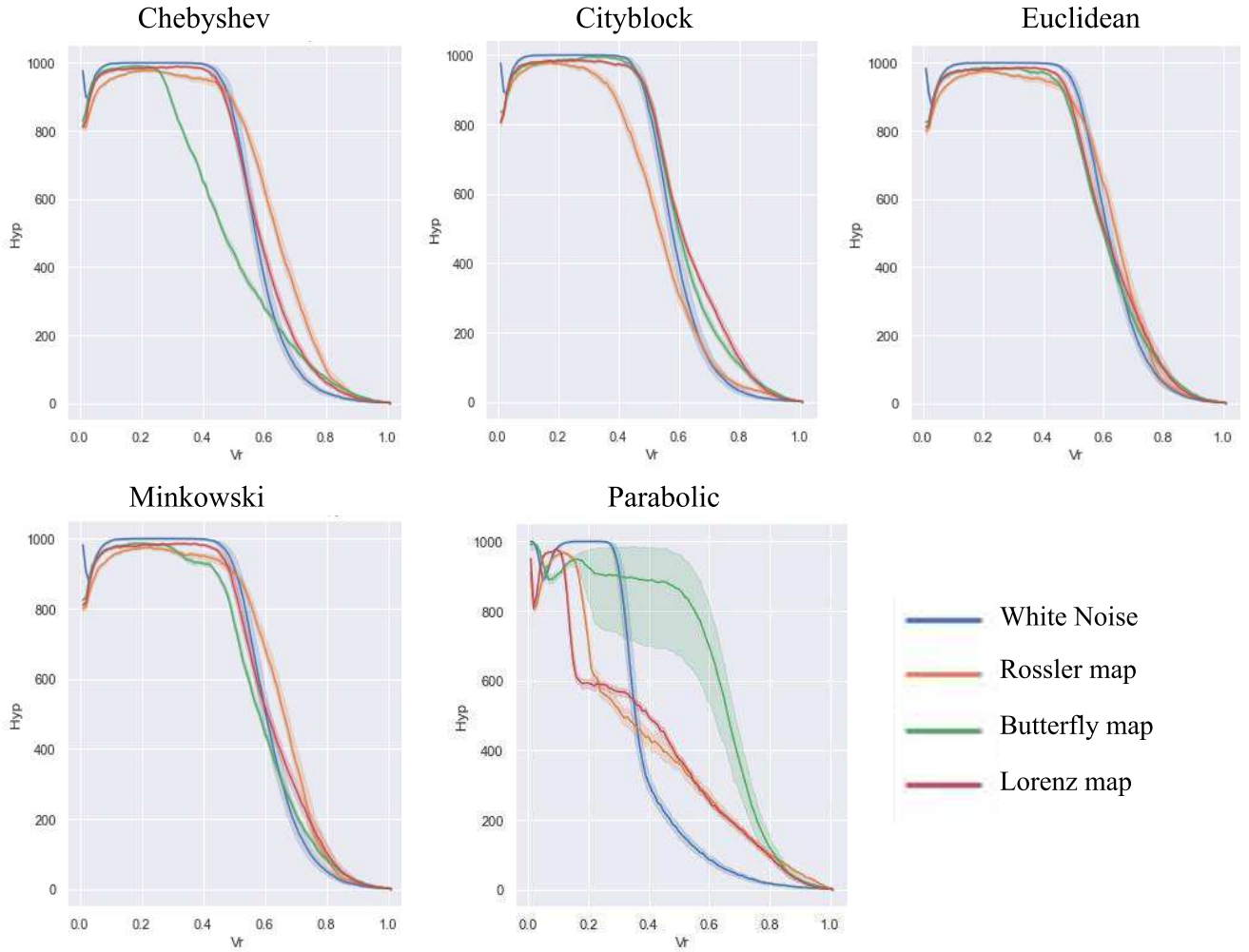


Figure 5: Analysis of the number of hyperedges versus parameter r , for three dynamical system (Lorenz map, Rossler map and Complex Butterfly map) and white noise. Each subplot represents the distance metric used to obtain the hypergraph.

5 Discussion

In this work we introduce a novel approach to study different datasets models using quantifiers obtained by the filtration evolution of the hypergraph. Particularly, we study the cases of five distributions of points and four dynamical systems. Our method shows the strength to extract information about the metric of the dataset, being able to distinguish and quantify all the distribution and the dynamical systems studied.

The study of the $\Delta^e(r)$ curves allow extract quantify in simple way the information extracted for the data. High values of the $\Delta^e(r)$ represent a low data clustering. When the radius r are small, the number of adjacent points tend to be zero, for example in cases as Normal or Uniform distribution $\Delta^e(r) = N_{data}$ –the ball of each point only contain itself. However, in other cases as Poisson, fractal distribution or Rossler map, for the initial radius $r = 0.01$ the $\Delta^e \ll N_{data}$, showing that the data are more clustered.

In all the example, with exception of fractal data, we can see that the initial values of $\Delta^e(r)$ remains constant as the r increase, drooping to zero at some critical r_c which depends of the distribution or dynamical system; the decrease in $\Delta^e(r)$ is maintained as r increases until its reach the value $r = 1$ –where a single hyperedge contain all points. These behaviour is expected because as the r increase, the number hyperedges containing the same points increase –remember when two hyperedges have the same points we consider only one. However, depending of the distance used between points, each

	White Noise	Complex Butterfly	Lorenz	Rosler
White Noise	0	967	1603	1498
Complex Butterfly	976	0	1405	925
Lorenz	1603	1405	0	784
Rosler	1498	925	784	0

Table 6: \mathcal{S} distance matrix for parabolic distance between dynamical system.

database present different curve shapes. For example, the lattice distribution present a staircase decay for the Chebichev and Cityblock distance. The fractal behaviour is very different from the others distribution due to why present picks and valleys as the value of r grows, this occurs due to the fractal nature of the distribution of the points where both clusters of points and large empty spaces exist in space. The difference between point distribution and dynamical systems depend in the metric used to generate the hypergraph. In both cases the Parabolic distance exhibit better results extracting information from the hypergraph topology which can be used to quantify and discern between them. The L^1 -Norm (\mathcal{L}) and Sobolev seminorm (\mathcal{S}) are presented as useful metrics for quantifying the curves $\Delta^e(r)$ obtained filtration method. Moreover, the pipeline introduced to measure a distance between two curves allows to unveil differences between the curves which cannot be obtained by comparing only the intrinsic values (both \mathcal{L} and \mathcal{S}) of each curve.

In this work we use the number of hyperedges as a quantifier of the hypergraph, however this not means that no exist other quantifier which gives different or complementary information about the hypergraph, for example obtain information about the vertices in the hyperedges. In the future works, we going to implement others quantifiers based in different attribution of the hypergraph.

Although in this work we have focused on the analysis of datasets of points, as described in section 2, this method applies to any dataset within a defined metric space such as signals, images, distributions, etc. In future work, we propose to extend this pipeline to the analysis of different data sets obtained from real life.

References

- [1] C. Berge and C. Berge. Graphes et hypergraphes. 1970. *Dunod, Paris*, 1967.
- [2] C. Berge. Graphs and hypergraphs. 1973.
- [3] S. Zhang, Z. Ding, and S. Cui. Introducing hypergraph signal processing: Theoretical foundation and practical applications. *IEEE Internet of Things Journal*, 7(1):639–660, 2019.
- [4] S. Barbarossa and M. Tsitsvero. An introduction to hypergraph signal processing. In *2016 IEEE International Conference on Acoustics, Speech and Signal Processing (ICASSP)*, pages 6425–6429. IEEE, 2016.
- [5] O. N. Temkin, A. V. Zeigarnik, and D. G. Bonchev. *Chemical reaction networks: a graph-theoretical approach*. CRC Press, 2020.
- [6] E. V. Konstantinova and V. A. Skorobogatov. Application of hypergraph theory in chemistry. *Discrete Mathematics*, 235(1-3):365–383, 2001.
- [7] S. Feng, E. Heath, B. Jefferson, C. Joslyn, et al. Hypergraph models of biological networks to identify genes critical to pathogenic viral response. *BMC bioinformatics*, 22(1):1–21, 2021.
- [8] S. Klamt, U-U. Haus, and F. Theis. Hypergraphs and cellular networks. *PLoS computational biology*, 5(5):e1000385, 2009.
- [9] A. Dutta Choudhury and A. S. Chowdhury. Champs: Cardiac health hypergraph analysis using multimodal physiological signals. In *2019 41st Annual International Conference of the IEEE Engineering in Medicine and Biology Society (EMBC)*, pages 4640–4645. IEEE, 2019.
- [10] Y. Zhu, X. Zhu, M. Kim, J. Yan, D. Kaufer, and G. Wu. Dynamic hyper-graph inference framework for computer-assisted diagnosis of neurodegenerative diseases. *IEEE transactions on medical imaging*, 38(2):608–616, 2018.
- [11] J. Guo, H. Li, X. Sun, L. Qi, H. Qiao, Y. Pan, J. Xiang, and R. Ji. Detecting high frequency oscillations for stereoelectroencephalography in epilepsy via hypergraph learning. *IEEE Transactions on Neural Systems and Rehabilitation Engineering*, 29:587–596, 2021.
- [12] J. Yu, D. Tao, and M. Wang. Adaptive hypergraph learning and its application in image classification. *IEEE Transactions on Image Processing*, 21(7):3262–3272, 2012.
- [13] M. R. Gauthama Raman, N. Somu, K. Kirthivasan, R. Liscano, and V. S. Sriram. An efficient intrusion detection system based on hypergraph-genetic algorithm for parameter optimization and feature selection in support vector machine. *Knowledge-Based Systems*, 134:1–12, 2017.
- [14] X. Ouvrard. Hypergraphs: an introduction and review. *arXiv preprint arXiv:2002.05014*, 2020.
- [15] I. S. Gradshteyn and I. M. Ryzhik. *Table of integrals, series, and products*. Academic press, 2014.

A Point Distribution Generation

Normal distribution

A discrete random variable x is said to have a Normal distribution if:

$$p(x, \mu, \sigma^2) = \frac{1}{\sigma\sqrt{2\pi}} e^{-\frac{1}{2} \left(\frac{x - \mu}{\sigma} \right)^2}$$

where μ is the location parameter, and it is going to be equal to the arithmetic mean and is the location parameter, and it is going to be equal to the arithmetic mean and σ^2 is the standard deviation. In our work for the different realisation we use the function `random.normal` in numpy Python package.

Poisson distribution

A discrete random variable x is said to have a Poisson distribution if:

$$p(x = k) = \lambda^k \cdot \frac{e^{-\lambda}}{k!}$$

Where k is an integer ($k \geq 0$) and λ is a positive real number. The Poisson distribution describes the probability of encountering exactly k events in a time span if the events occur independently at a constant rate λ . To generate the distribution we use the function `random.poisson` in numpy Python package.

Uniform distribution

The uniform Distribution is given by the formula:

$$p(x, a, b) = \begin{cases} \frac{1}{b-a} & \text{for } a \leq x \leq b \\ 0 & \text{for } x < a \text{ or } x > b \end{cases}$$

In our work we use $a = -1$ and $b = 1$ and use the function `random.uniform` in numpy Python package.

Lattice array

A lattice is an ordered array of points describing the arrangement of particles that form a crystal. In our work we build the lattice defining a 3-dimensional cube and putting the data in a \mathbf{x} -distance position.

Fractal array

For the fractal array we generate $N = 1000$ 3D points. The coordinates $\mathbf{X} = [x^1, x^2, x^3]$ of the each point follows the next pipeline. For each coordinate x^l we generate a vector of length $L = 100$, $\mathbf{x}^l = \{x_1^l, \dots, x_{100}^l\}$ with x_i^l randomly chosen between $\{0, 3\}$ –for example $\mathbf{x}^1 = \{0, 3, 0, 0, 0, 3, 0, \dots, 0\}$ –, then we measure the x^l values as:

$$x^l = \sum_{i=1}^L \frac{x_i^l}{4^i} \quad \text{for } l = 1, 2, 3$$

B Dynamical System Generation

Lorenz attractor

The Lorenz attractor is defined as the dynamical system governed by the following system of equations:

$$\begin{cases} \frac{dx}{dt} = \sigma(y - x) \\ \frac{dy}{dt} = -xz + rx - y \\ \frac{dz}{dt} = xy - bz \end{cases}$$

where we take the usual values $\sigma = 10$, $r = 284$, $b = 8/3$ of the parameters. With the following initial conditions $x_0 = 0$, $y_0 = -0.01$ and $z_0 = 9$

Rössler attractor

The Rössler attractor is the attractor of the Rössler system, a system of three nonlinear ordinary differential equations

$$\begin{cases} \frac{dx}{dt} = -y - z \\ \frac{dy}{dt} = x + ay \\ \frac{dz}{dt} = b + z(x - c) \end{cases}$$

where we take the usual values of the parameters $a = b = 0.2$, $c = 5.7$. With the following initial conditions $x_0 = -9$, $y_0 = 0$ and $z_0 = 0$.

Complex butterfly attractor

The Complex butterfly attractor is a system of three nonlinear ordinary differential equations:

$$\begin{cases} \frac{dx}{dt} = a(y - z) \\ \frac{dy}{dt} = -z \operatorname{sgn}(x) \\ \frac{dz}{dt} = |x| - 1 \end{cases}$$

where we take the usual values of the parameters $a = 0.55$, $c = 5.7$. With the following initial conditions $x_0 = 0.2$, $y_0 = 0$ and $z_0 = 0$.